ALMA BAND 2+3
FORE-OPTICS DESIGN REPORT

ISSUE 2.0 (Final Review)

Prepared by: Renzo Nesti (1), Fabrizio Villa (2) and Luca Terenzi (2)
(1) INAF/OAA – Largo Enrico Fermi 5, I-50125 Firenze, Italy
(2) INAF/IASF.bo – Via P. Gobetti 101, I-40129 Bologna. Italy

Checked by: Renzo Nesti (WP manager)

ABSTRACT

This report describes a study of the ALMA band 2+3 (67-116GHz) Fore-Optics (FO) with the aim to investigate the possibility to implement the fore-optics at cold, i.e. inside the cartridge at 15K. We studied the performances of the FO with ALMA antenna and different feed designs. We compare performances with the warm scheme of the FO as implemented in the band 3 cartrdige.

1 SOMMARIO

2 INTRODUCTION

The fore-optics for ALMA is necessary for matching the F/# of the ALMA antenna with the F/# of the horn as well as to match the Cassegrain focal point with the phase centre of the horn located at cold inside the cryostat. For band 2 a warm lens system was studied as reported while for band 3 a warm mirror system was implemented [1]. Here, with this preliminary study, we investigate the possibility to design a mirror system that can be positioned at cold. The advantage to have a cold optics are

1. Minimization of the losses (i.e. added noise) and the contribution due to the spillover.
2. Minimization of the degradation of the sensitivity due to temperature fluctuations of the fore-optics
3. Reduction of the straylight signal due to spillover losses generated along the fore-optics optical path

The main disadvantage is to mitigate the allowable volume with the optical requirements.

3 Opto-mechanical Requirements

In order to start with the study a 3D mechanical sketch based on the band 2 cartridge drawings was implemented in Autodesk Inventor and reported in Figure 1.

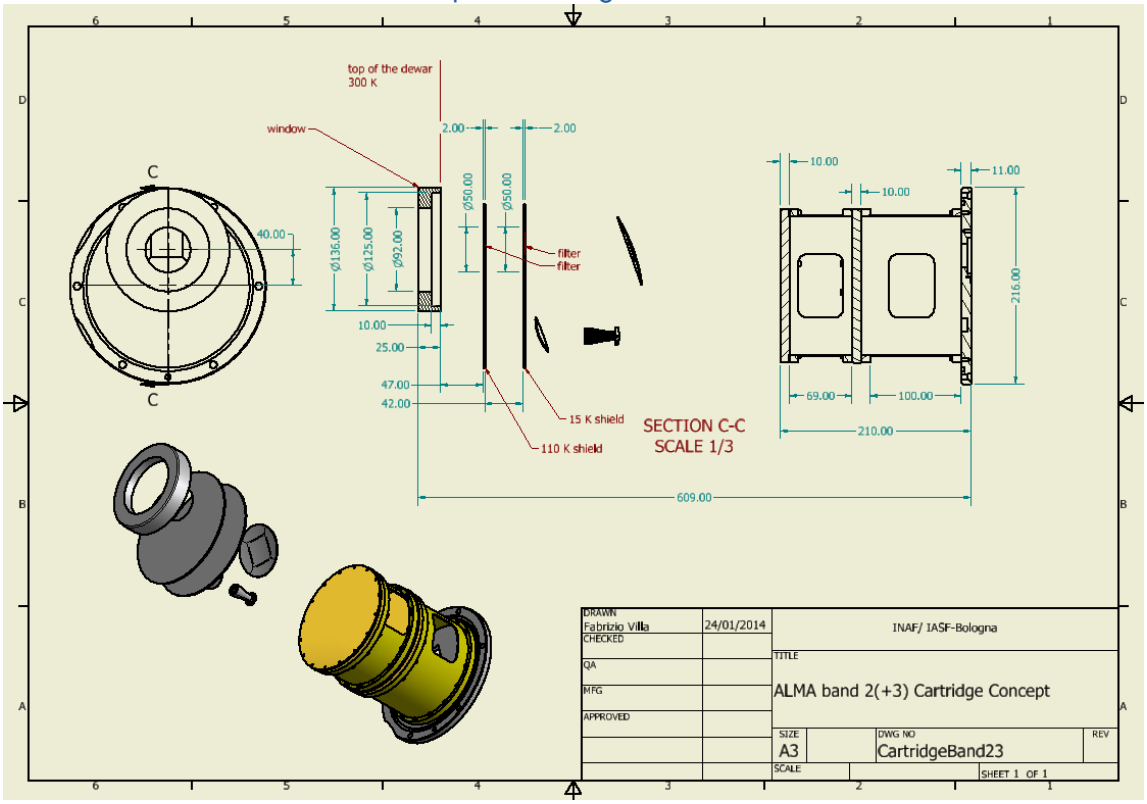

Figure 1. Mechanical sketch of the ALMA band 2 Cartridge as derived from documentation and from solid model by STFC /RAL

As optical requirements, in addition to those reported in [2], we set the followings:

Table 1 opto-mechanical requirements

Band 2+3 Opto-mechanical requirements	
Cassegrain focal point (above cryostat)	70 mm
Band 2 chief ray tilting:	2.48 deg
Half- angle subtended by sub reflector:	3.58 deg
Frequency range band 2+3	67 – 116 GHz
Central frequency band 2+3	91.5 GHz

5 Design Approach and Assumptions

FO Design guidelines are stated in Chapter 2.2 of the ALMA front-end design report [3] and listed (in bold) and commented hereafter:

- **Gaussian beam approximations are used to design the active optics surfaces. These approximations are supplemented with PO analysis [RD3, RD4, and RD5].**
    - The Gaussian beam approximation (GBA) has been introduced to design the FO of the band 2+3. It should be noted that at these frequency the PO analysis is mandatory since the performances cannot be fully determined with the GBA.
- **Secondary mirror illumination taper is -12 dB for Gaussian beam approximations, which is about –10 dB in the PO analysis. This produces a reasonable compromise between aperture efficiency and spill-over loss as well as between interferometer and single dish observing modes beam requirements.**
- **Cold reflective optics (mirrors) are used where possible to reduce noise. This can be fulfilled for most of the bands. Mirror reflection angles are minimized to decrease the cross-polarization levels.**
    - Since the design of the cold optics for the band 2+3 is challenging reflection angles are driven by the allowable space in the cartridge instead of cross-polar level.
- **During the operations, the telescope secondary mirror position can be adjusted to refocus the telescope from one band to another.**
    - No adjustment of the telescope secondary mirror has been assumed for overall performance calculations.

The beam clearance of 5 waist radii at the lowest frequency of each band, except band 1, (Gaussian beam approximation) has been adopted for signal beams to assure that truncation loss is below 1%. This is the driving requirement for size of mirrors, windows and infrared filters, as well as other aperture limiting elements.

- This requirement cannot be fulfilled so that it has not assumed as a driver. However beam truncation effects have been evaluated.

- **Corrugated horns have been adopted as mixer feed design.**
    - Corrugated horn has been used.

- **Optics interface with telescope is clearly defined by beam parameters at the telescope focal plane.**

    - Apart from the edge taper, we used the location of the nominal Cassegrain focus and the direction of the chief ray for band 2.

- **Each receiver will point at the center of the subreflector; misalignment tolerances can only give an efficiency loss of 1% at zenith, with a further 2 % loss over the elevation angle range.**

    - The exact pointing of the beam out from the FO has not been optimized. At this stage we assumed that the nominal chief ray inclination for band 2 fulfil this requirement in the GO approximation.

6 THERMAL CONSIDERATIONS AND NOISE BUDGET

The estimation of the differences between the optics (here assumed composed by two mirrors) at ambient temperature (300K) and at cryogenic temperature (15K) is reported here. We assumed the mirrors composed by Aluminium 6061 and we evaluated the thermal emission at both temperatures and at various wavelengths.
We applied the formula reported in [4]

$$\frac{\Delta T}{T_{sys}} = (L-1)\left(\frac{T_{phys}}{T_{sys}} + 1\right)$$

Where L (reflection loss) is evaluated from:

$$1 - \frac{1}{L} = 4\sqrt[2]{\frac{\pi \varepsilon_0 \nu}{\sigma}}$$

Results show that the differences in the conductivity from room to cryogenic temperatures have a limited impact on the mirror emission, while the main contribution is due to the re-emission due to the physical temperature of the mirrors. This gives about an order of magnitude worse noise at ambient with respect to cryogenic temperature. Since the L can be small for optical finished surfaces, the absolute value of the noise increase is to be evaluated in the overall noise budget.

From the fractional increment of noise calculated, the RF noise induced by the optics has been evaluated as function of frequency in the following case:

- Receiver with Tnoise = 50K
- Receiver with Tnoise = 30K

An additional evaluation was performed to estimate the noise temperature variation caused by a 2K physical temperature fluctuations of the mirrors exposed to room environment. The result is a variation of the order of few mK to be compared with the overall stability budget. Results are reported in Table 2, in
Figure 2.

Table 2. noise temperature increment due to the FO at cold and warm. The estimation of the noise temperature fluctuation due to a variation of 2K for the FO at warm is also estimated.

Freq	dT/Tsys (15K)	dT/Tsys (300K)	dT/Tsys (298K)	Tnoise fluctuation
		Band 2+3		
67 GHz	0.001672	0.015534	0.015445	4.44 mK
91 GHz	0.001949	0.018109	0.018005	5.17 mK
116 GHz	0.002200	0.020451	0.020334	5.84 mK

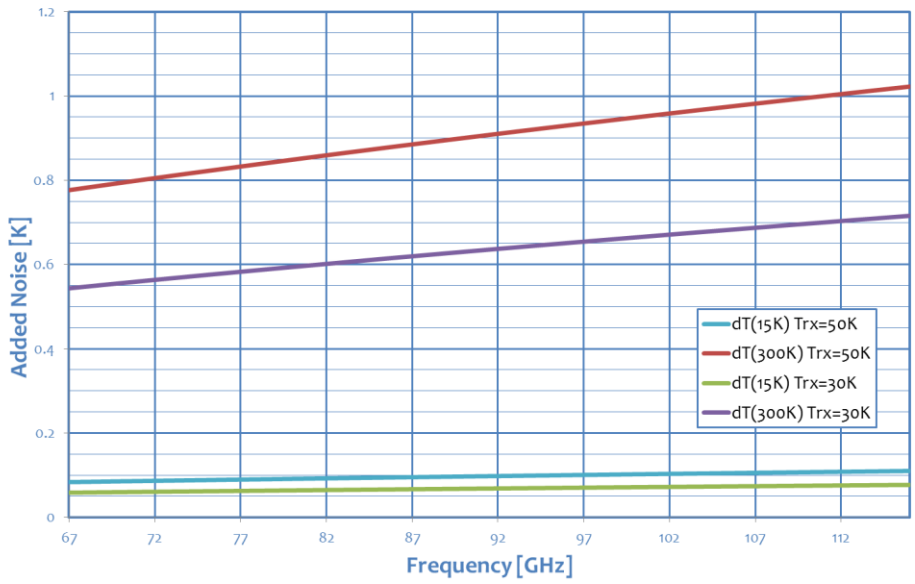

Figure 2. Added noise due to the Fore Optics at cold and at warm with different radiometer noise (30 and 50 K).

The following scheme reports the noise budget for the different cases evaluated in this study. It is noticed that the gain in using a cold FO is of about one order of magnitude. However the worst case (warm FO and 50K radiometer noise) gives a noise contribution of about 1K that becomes 0.1K if a cold optics is implemented. From the point of view of the fluctuations, the cold optics offer supreme noise stability w.r.t the warm optics because of the controlled thermal environment that gives negligible added fluctuations.

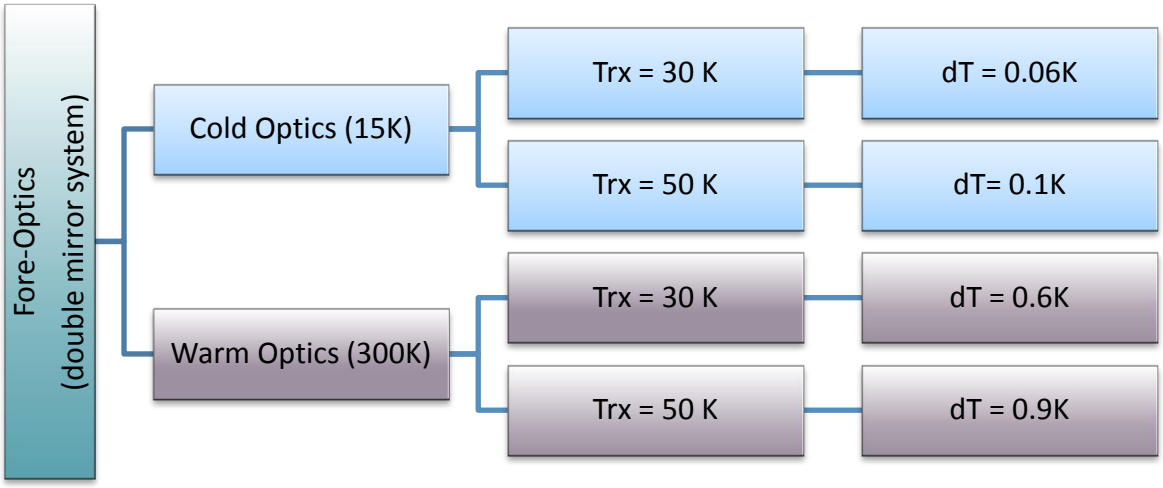

7 "REFERENCE" PERFORMANCES

We calculated the gain and the efficiency using (1) a Gaussian equivalent feed with a taper of -12 dB @ 3.58 deg. and (2) a pure HE11 hybrid-mode circular waveguide with 32mm of aperture radius to obtain a corrugated horn like pattern with approx. the same edge taper of the Gaussian equivalent feed. In Figure 3 the radiation patterns for the two cases are reported.

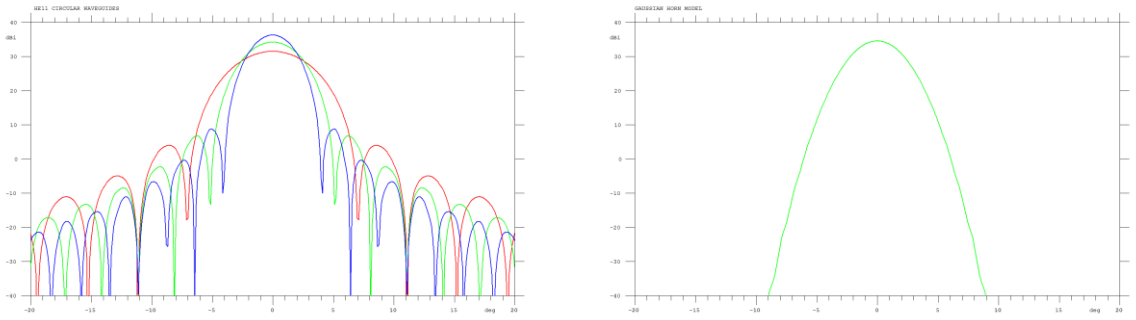

Figure 3: Horn models used for the calculation of 'reference' performances. The radiation pattern of a pure HE11 circular waveguide pattern is shown on the left at 67 GHz (red), 91.5 GHz (green) and at 116 GHz (blue). On the right the pure Gaussian radiation pattern is plotted at 91.5 GHz. Since it is defined by the taper angle the pattern is equal also at the other two frequencies.

The horn pattern was propagated through the sub-reflector and the main-reflector to calculate the final ALMA antenna pattern in the ideal case so that the blockage, the struts diffractions, the mirror's deformations and roughness were neglected. We estimated the total efficiency in both cases with methods reported in the following paragraphs.

Table 3: Reference performances. (1) equivalent parabola is the case of the ALMA antenna with perfectly uniform illumination from which the total efficiency is calculated (see text for details).

	Co-polar Directivity	X-pol Directivity	Total Efficiency	Total Spillover	Spill Efficiency	Spill+pol Efficiency	Pol Efficiency
Gaussian							
67 GHz	77.40 dBi	34.30	78%	7.8%	94%	94%	1
91.5 GHz	80.11 dBi	36.95	78%	7.8%	94%	94%	1
116 GHz	82.18 dBi	38.98	78%	7.8%	94%	94%	1
HE11							
67 GHz	77.01 dBi	34.85	71%	24%	77%	77%	1
91.5 GHz	80.22 dBi	37.15	80%	6.5%	95%	95%	1
116 GHz	81.53 dBi	37.21	67%	2.7%	99%	99%	1
Equivalent Parabola (1)							
67 GHz	78.50 dBi	N/A	1	0	1	1	1
91.5 GHz	81.21 dBi	N/A	1	0	1	1	1
116 GHz	83.27 dBi	N/A	1	0	1	1	1

7.1 CALCULATION OF LOSSES AND EFFICIENCIES.

We define the following pattern quantities (according to GRASP convention):

P_{cp} the co-polar radiation pattern

P_{xp} the cross-polar radiation pattern

P_{pwr} the power radiation pattern, i.e. the pattern with the amplitude $\sqrt{|P_{cp}|^2 + |P_{xp}|^2}$ and zero phase everywhere.

The maximum pattern directivity is defined as

$$D = D_0 \cdot \eta = \left(\frac{4\pi A}{\lambda^2}\right) \cdot \eta$$

where A is the antenna aperture area and η is the **total efficiency**. For ALMA the aperture area is calculated as the geometrical area form $A = \frac{\pi d^2}{4} = 113.097 m^2$. It can be calculated alternatively form the solid angle subtended by the subreflector (as seen from feed) and equivalent parabola focal length as $A = \Omega_{sub} \cdot {f_{eq}}^2 = 2\pi(1 - \cos(3.58°)) \cdot 96^2 = 112.998 m^2$. For the calculations, a geometrical area of $A = 113 m^2$is taken as reference.

The directivity D_0 is the directivity of an antenna with aperture area equals to ALMA aperture area with perfect uniform illumination and zero spillover and zero cross polarization, so that the total efficiency is $\eta = 1$.

In the 'real' case the total efficiency η is calculated once the 'real' directivity is estimated from simulation from

$$\eta = \frac{D}{D_0}$$

As in [5], the total efficiency is the product of several efficiencies:

$$\eta = \eta_{amp} \cdot \eta_{phase} \cdot \eta_{pol} \cdot \eta_{spill}$$

The method to evaluate the efficiencies is reported in the following paragraph, limited to the spillover η_{spill} and polarization η_{pol} efficiencies.

Moreover we calculated the effective area in the case of the equivalent parabola is using equation (5.3) in [4]:

$$A = {f_0}^2 \Omega$$
$$\Omega = 2\pi(1 - \cos\theta_m)$$

Were θ_m is the semi-angle subtended by the equivalent parabola (3.58 deg) and $f_0 = 96000\, mm$ is the total focal length. From the effective area we then estimated the maximum directivity as

$$D_0 = \frac{4\pi A}{\lambda^2}$$

7.1.1 Spillover and Polarization Efficiencies

According to [6], the fore-optics Beam efficiency is calculated from radiation pattern within cone with semi-angle = 3.58:

$$\eta_{spill} = \frac{\int_{\Omega_{sub}} P_{pwr}(\Omega)\, d\Omega}{\int_{4\pi} P_{pwr}(\Omega) d\Omega} = \frac{\int_0^{2\pi}\int_0^{3.58} P_{pwr}(\theta,\phi)\sin\theta\, d\theta d\phi}{4\pi}$$

Cross polar effects are evaluated trough the efficiency calculation as follows:

$$\eta_{pol} = \frac{\int_{\Omega_{sub}} P_{cp}(\Omega) d\Omega}{\int_{\Omega_{sub}} P_{pwr}(\Omega) d\Omega} = \frac{\int_0^{2\pi}\int_0^{3.58} P_{cp}(\theta,\phi)\sin\theta\, d\theta d\phi}{\int_0^{2\pi}\int_0^{3.58} P_{pwr}(\theta,\phi)\sin\theta\, d\theta d\phi}$$

We derive then that the product of spillover and polarization efficiencies can be evaluated by

$$\eta_{spill+pol} = \eta_{spill} \cdot \eta_{pol} = \frac{\int_0^{2\pi}\int_0^{3.58} P_{cp}(\theta,\phi)\sin\theta\, d\theta d\phi}{4\pi}$$

7.1.2 NOISE DUE TO BEAM TRUNCATION

For the FO, the noise added by truncation effects is evaluated by the spillover power calculated for the two mirrors of the FO. The Spillover power is evaluated from PO calculation as the power that does not hit the mirrors. Following GRASP convention, the spillover is calculated as: $spill = 10log_{10}\frac{4\pi}{W}$, where W is the total power hitting the reflector so that

$$W = \int_{rfl} P_{pwr} d\,\Omega$$

Starting from the calculation of the antenna temperature we can estimate the noise added by the spillover by imposing that the power that does not hit the reflectors sees an environment at T_{env}, while the power hitting the reflectors sees a temperature coming from sky, T_{sky}.

$$T_A = \frac{1}{4\pi}\int_{4\pi}(P_{pwr}\cdot T) d\,\Omega = \frac{1}{4\pi}\int_{rfl}(P_{pwr}\cdot T_{sky}) d\,\Omega + \frac{1}{4\pi}\int_{(4\pi-rfl)}(P_{pwr}\cdot T_{env}) d\,\Omega$$

$$T_A = \frac{1}{4\pi}T_{sky}\int_{rfl} P_{pwr} d\,\Omega + \frac{1}{4\pi}T_{env}\int_{(4\pi-rfl)} P_{pwr} d\,\Omega = \left(\frac{W}{4\pi}\right)\cdot T_{sky} + \left(1-\frac{W}{4\pi}\right)\cdot T_{env}$$

We define here the added noise as the

$$T_{trunc} = T_{spill} = \left(1-\frac{W}{4\pi}\right)\cdot T_{env}$$

8 CONFIGURATION 1 – CONJUGATE PARABOLIC MIRRORS

No further studies of this configuration were performed. For an easier reading of the document this part has been omitted. Please refer to *ALMA band 2+3 fore-optics design report ver 1.1* for reference (Mid-term review).

9 CONFIGURATION 2: 'STANDARD MIRROR DESIGN

In this case a standard technique in quasi-optical systems (Gaussian beam analysis) has been applied. In total **six configurations** were analysed for the 'standard mirror design' all based on a two ellipsoidal reflector arrangement. Starting from the feed, the optics has been designed in order to obtain approximately a -12 dB taper at the ALMA subreflector matching at the wavefront radius of the beam with the curvature radius of the subreflector mirror. In addition the constraints due to the cartridge, cryostat, and location of the Gregorian focus has been taken into account. The parameters of the six configurations are reported in Table 4. The first four configurations did not fit the cartridge envelope so that the RF study was concentrated on ver.5 and its modification ver.5bis. The scheme and the layout of the configurations are reported Figure 4.

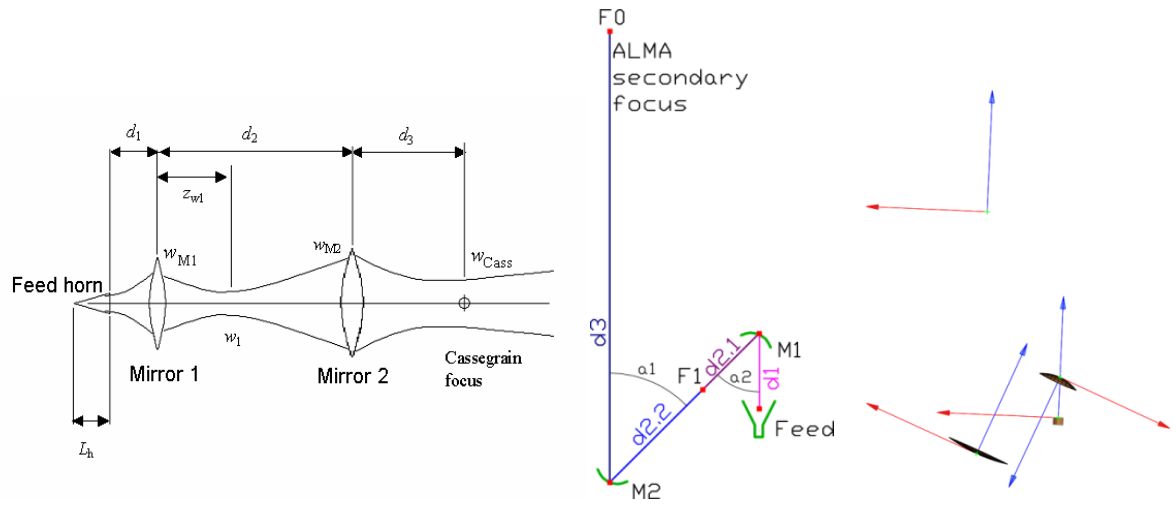

Figure 4: Layout (center) of the "standard mirror design", according with the ALMA fore optics baseline representation scheme (left). The optics is composed by two off-axis ellipsoidal mirror, M1 and M2 whose location has been settled by the cartridge allowable volume and location of the nominal band 2 Cassegrain focus. On the right one of the FO version implemented in GRASP software.

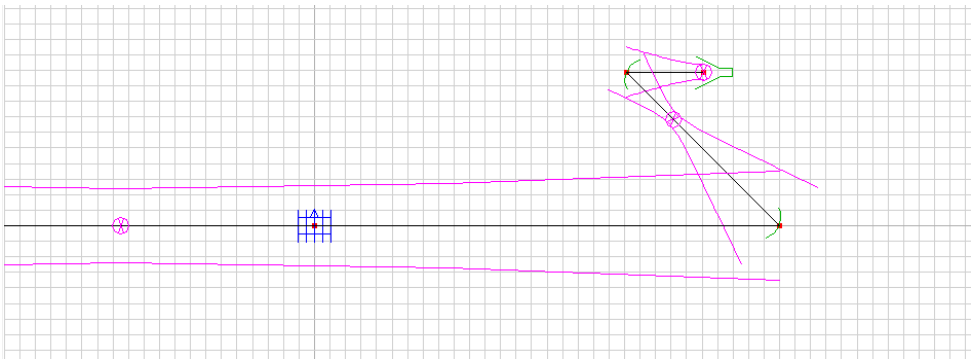

Figure 5: Layout of the Fore Optics ver.5 . The red dot on the blue grid represent the location of the nominal Cassegrain focus for the band2 cartridge system. The magenta curves are the level at -12.00 dB of the beam propagated from the feed (w0 = 4) through the two reflectors.

Table 4: Parameters of the five versions considered in this study.

	Ver. 1	Ver. 2	Ver. 3	Ver. 4	Ver. 5	Ver. 5bis
			Input parameters			
d1			50 mm	50 mm	50 mm	50
d2.1	100 mm	50 mm	50 mm	50 mm	50 mm	50
d2.2	100 mm	50 mm	100 mm	100 mm	90 mm	90
d2 = d2.1+d2.2	200	100mm	150mm	150mm	140mm	140mm
d3	300 mm	300 mm	300 mm	350 mm	300 mm	300mm
Feed waist	4mm @91.5 GHz					
			Derived "Optimized" parameters			
			Mirror 1			
R1	60 mm	43.356 mm	50 mm	50 mm	50 mm	50mm
R2	100 mm	60.981 mm	50 mm	50 mm	50 mm	50mm
F	37.5 mm	25.340 mm	25 mm	25 mm	25 mm	25mm
			Mirror 2			
R1	250.436 mm	99.261 mm	123.180 mm	120.786 mm	109.495 mm	107.491mm
R2	250.436 mm	141.493 mm	688.925 mm	880.124 mm	502.523 mm	462.921mm
f	125.2178 mm	58.337 mm	104.496 mm	106.210 mm	89.905 mm	87.235mm

We report in the following paragraphs the detailed study on the configuration 5 (see Figure 5), and its modification 5bis.

9.1 VERSION 5

The fore optics was further analysed using full PO/PTD analysis to calculate the field at the aperture cryostat window. The use of PO/PTD allowed to calculate the spillover of the reflectors (see Table 5) and the field at the mirror aperture (see Figure 6). The spillover has been used to estimate the noise added by truncation of the beam.

Table 5. Fraction in percentage of Power that does not hit the M1 and M2 mirrors. Total spillover is the sum of the two spillover. The added noise has calculated considering a 15 K environment. Noise added by beam truncation on window has been estimated considering 300 K environmental Temperature.

Frequency	Spillover M1	Spillover M2	Spillover M1+M2	Spillover window	Spillover total	Mirror Truncation [K]	Window Truncation [K]
67.0 GHz	2.18%	9.86%	12.04%	2.27%	14.3%	1.8K	6.81K
91.5 GHz	0.13%	4.06%	4.19%	0.87%	5.1%	0.6K	2.61K
116.0 GHz	0.005%	1.75%	1.76%	0.32%	2.1%	0.3K	0.96K

The Spillover at window level has calculated introducing a dummy reflector at the window location and with the same dimensions of the window itself. In this way we can estimate the total power that reach the window.

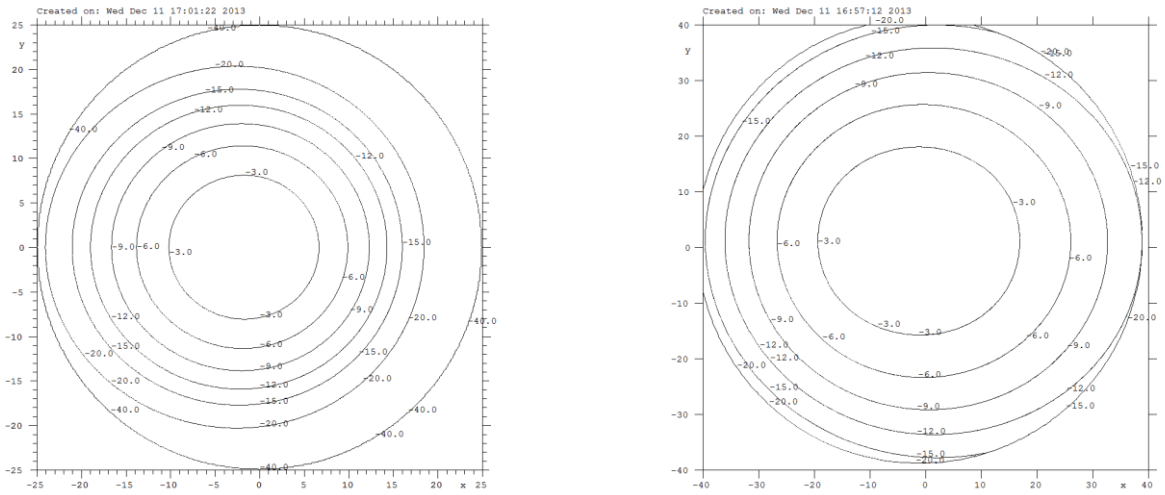

Figure 6: Power of the Electrical field on M1 (left) and M2 (right) surfaces. Level on the reflector rim is not representative of the edge taper.

The far-field pattern of the optics has been calculated with full PO/PTD analysis considering the fore-optics alone in the nominal Band-2 focus.

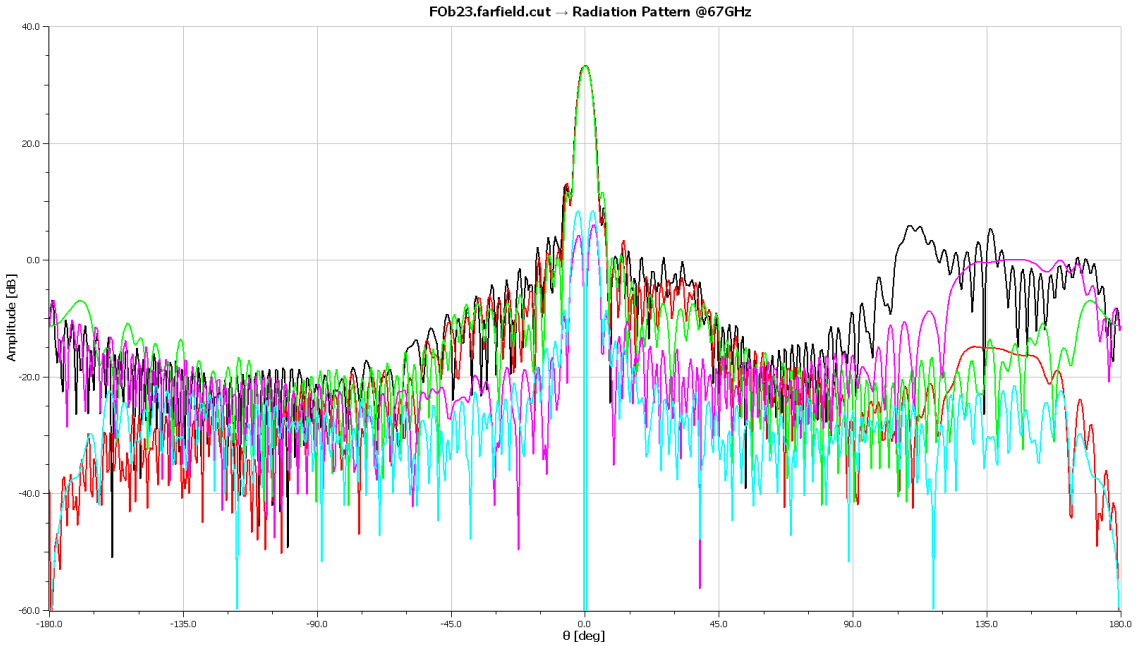

Figure 7. Far field radiation pattern @ 67 GHz of the Fore-Optics V5 with Gaussian feed with W0 = 4 mm. Black: E-plane copolar field; red: I-plane copolar field; green: H-plane copolar field; magenta: I-plane crosspolar field. Cyano: H-plane crosspolar field.

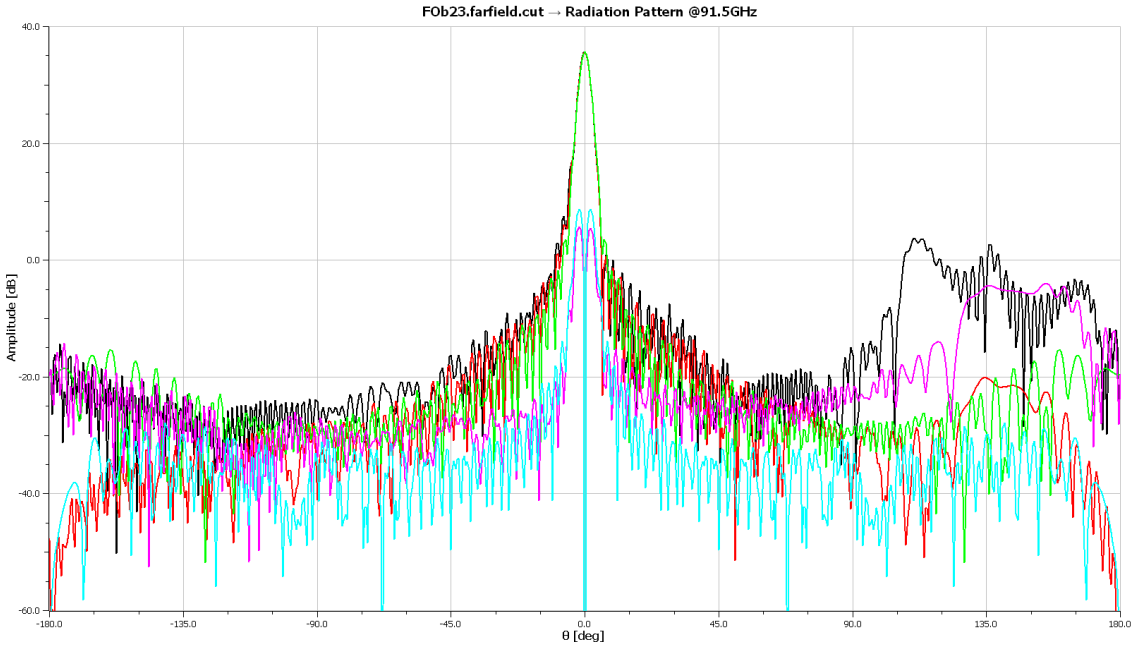

Figure 8. Far field radiation pattern @ 91.5 GHz of the Fore-Optics V5 with Gaussian feed with W0 = 4 mm. Black: E-plane copolar field; red: I-plane copolar field; green: H-plane copolar field; magenta: I-plane crosspolar field. Cyano: H-plane crosspolar field.

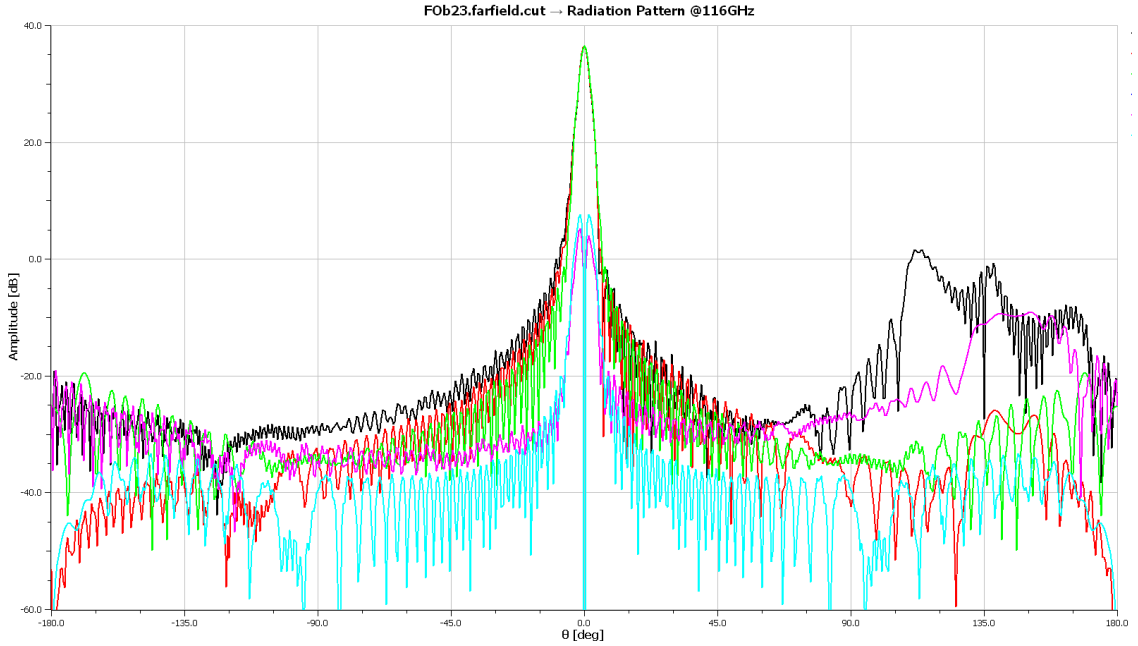

Figure 9. Far field radiation pattern @ 116 GHz of the Fore-Optics V5 with Gaussian feed with W0 = 4 mm. Black: E-plane copolar field; red: I-plane copolar field; green: H-plane copolar field; magenta: I-plane crosspolar field. Cyano: H-plane crosspolar field.

The Fore-optics V5 (stand-alone) has been coupled with the ALMA antenna. The radiation pattern from the fore optics using Gaussian feed definition has been considered as a source for the PO analysis with the sub-reflector and main-reflector of ALMA. Here the mirrors were considered ideal so that as perfect conducting surfaces, without roughness, neglecting also the effect of blockage and of the sub-reflector support structure.

PO/PTD method has been selected for the sub-reflector analysis, while for the main reflector analysis only PO method has been applied. The results are hereafter reported.

Table 6: Calculated parameters with fore-optics V5 and different horn models. The total efficiency includes also the illumination (in amplitude and phase) efficiency with respect to perfect uniform illumination function of the ALMA antenna. (1) The spillover has been derived from PO calculation; the total spillover is the percentage of the power hitting the sub and the main reflectors. The sub reflector spillover is the power percentage hitting the sub reflector (this number is comparable with the spillover efficiency).

	Directivity	Cross-polar Discrimination	Total and sub Spillover (1)	Spill Efficiency	Pol+spill Efficiency	Total efficiency
Gaussian W0 = 4mm						
67 GHz	76.6 dBi	-26.76 dB	Total: 78.47% Sub: 79.81%	80.30%	80.03%	64.71%
91.5 GHz	79.42 dBi	-27.49 dB	Total: 89.34% Sub: 90.94%	90.27%	90.04%	66.22%
116 GHz	81.56 dBi	-29.25 dB	Total: 92.50% Sub: 94.47%	94.20%	94.05%	67.45%
INAF Linear horn						
67 GHz	76.40 dBi	-27.21 dB	Total: 74.96% Sub: 76.23%	76.54%	76.31%	61.66%
91.5 GHz	78.97 dBi	-29.42 dB	Total: 78.13% Sub: 79.64%	78.94%	78.81%	59.70%
116 GHz	80.99 dBi	-29.99 dB	Total: 80.63% Sub: 82.66%	82.56%	82.42%	59.16%
INAF Profiled horn						
67 GHz	76.54 dBi	-26.92 dB	Total: 77.42% Sub: 78.76%	79.30%	79.05%	63.68%
91.5 GHz	79.12 dBi	-29.18 dB	Total: 78.47% Sub: 79.96%	79.42%	79.28%	61.80%
116 GHz	81.23 dBi	-32.25 dB	Total: 78.67% Sub: 80.58%	80.71%	80.57%	62.52%
IRAM profiled horn						
67 GHz	76.37	49.19	Total: 74.37% Sub: 75.62%	75.89%	75.67%	61.21%
91.5 GHz	79.01	49.96	Total: 78.33% Sub: 79.84%	79.10%	78.96%	60.27%
116 GHz	81.24	51.89	Total: 81.57% Sub: 83.51%	83.44%	83.30%	62.67%

The field on sub-reflector has been calculated in order to evaluate the taper. As expected, the worst taper level is at 67 GHz and it is 12 dB as required by ALMA top-level specifications. Due to the change of the beam from FO with frequency a constant illumination function over the bandwidth is not guaranteed with this design.

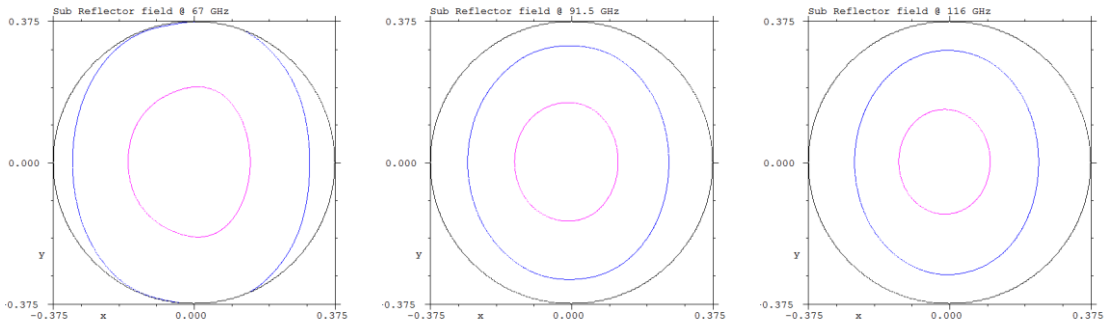

Figure 10. Field on the sub reflector after reflection with FOv5 and Gaussian feed. Magenta and Blue contours are respectively the -3 dB and -12 dB levels. The circle in Black is the sub-reflector rim. Axis units are meters.

9.2 FAR FIELD PATTERN

The main beam far field patterns were calculated using PO/PTD analysis as usual.

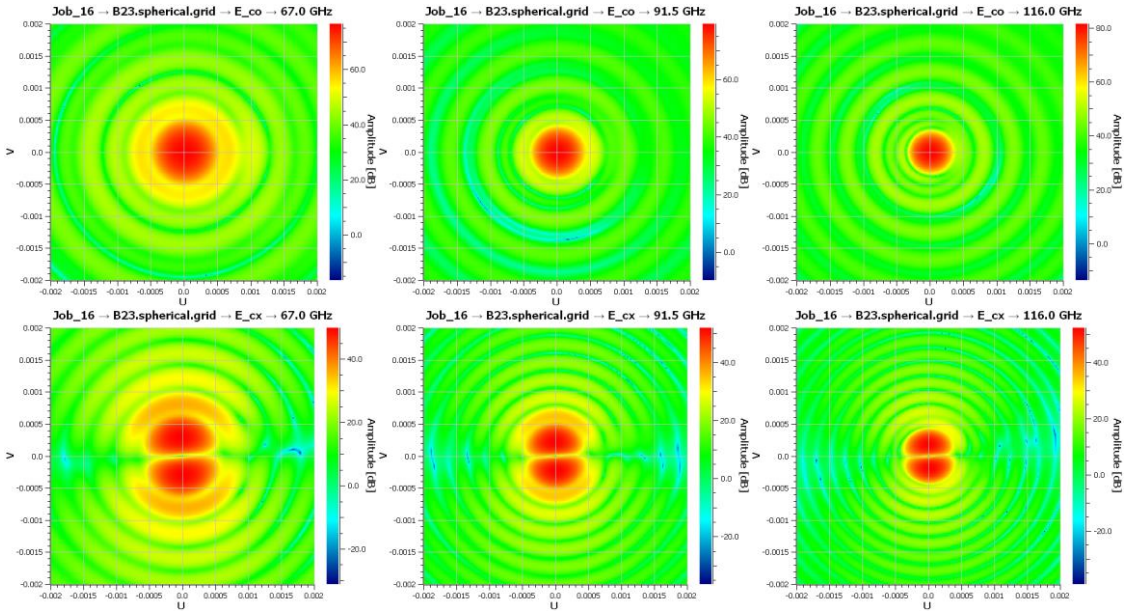

Figure 11. Main beam pattern with FO ver. 5 and pure Gaussian feed model. Upper: co-polar main beam @ 67, 91.5, and 116 GHz. Bottom: cross-polar beam @ 67, 91.5, and 116 GHz.

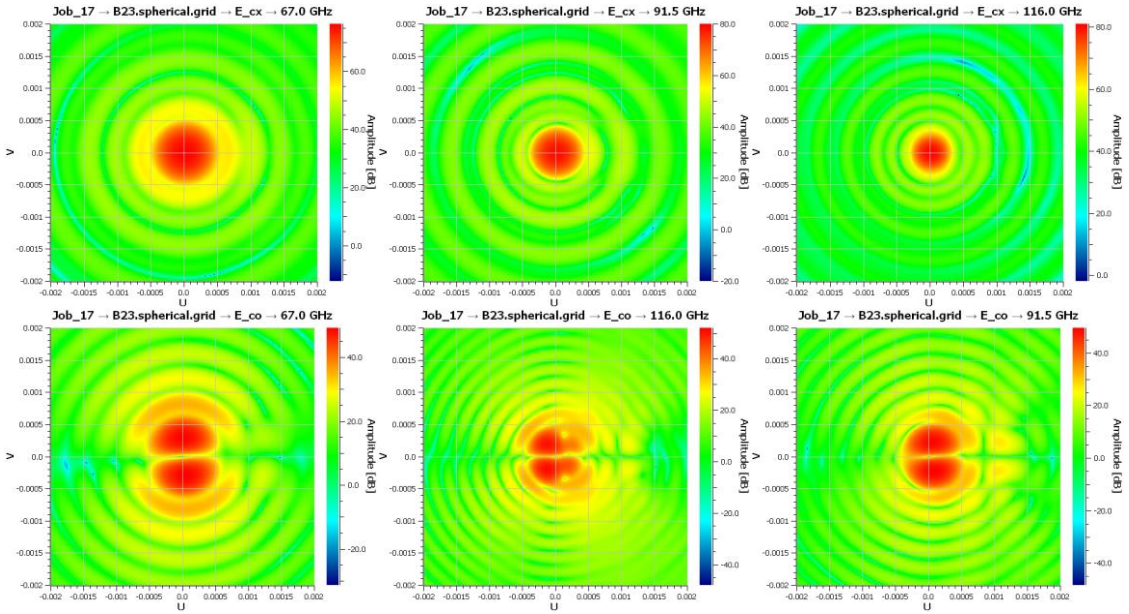

Figure 12. Main beam pattern with FO ver. 5 and INAF linear feed model. Upper: co-polar main beam @ 67, 91.5, and 116 GHz. Bottom: cross-polar beam @ 67, 91.5, and 116 GHz.

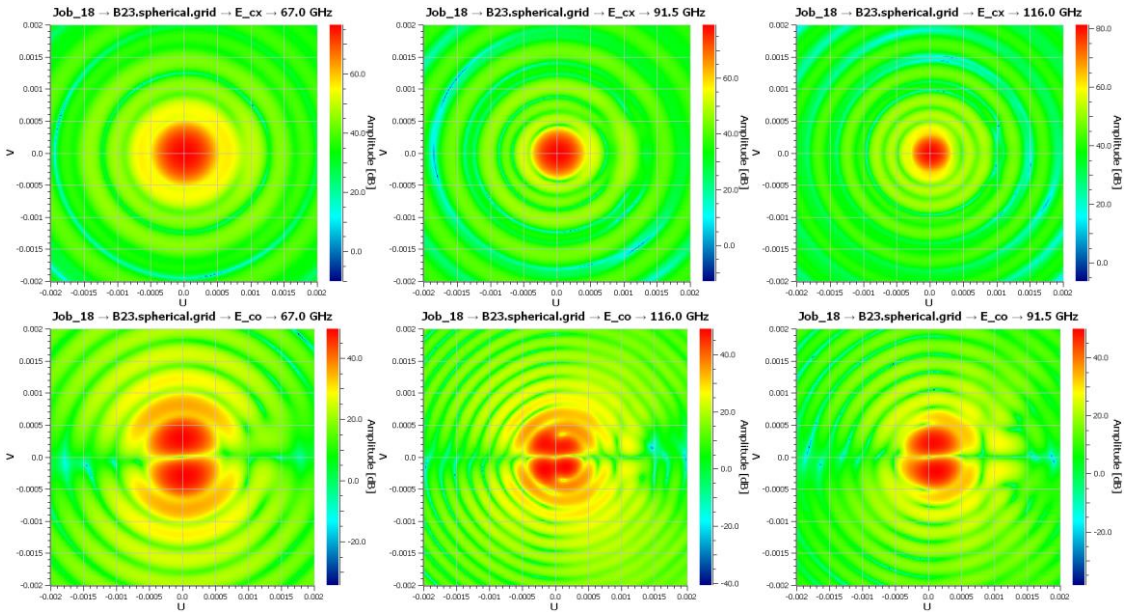

Figure 13. Main beam pattern with FO ver. 5 and INAF sin2 profiled feed model. Upper: co-polar main beam @ 67, 91.5, and 116 GHz. Bottom: cross-polar beam @ 67, 91.5, and 116 GHz.

In the table below we report the main beam parameter as derived from the maps. A Gaussian fit has been performed to carry out the angular resolution and ellipticity of beams. Moreover a depolarization factor has been evaluated from the beam maps expressed in stokes parameters, S_Q, S_U, S_V, S_I as:

$$Dep\% = \left(1 - \frac{\sqrt{S_Q^2 + S_U^2 + S_V^2}}{S_I}\right) \cdot 100$$

Although this is not an usual 'ALMA' parameter, it is useful because represents the percentage of the signal lost due to polarization mismatch of the beam (obviously it is related to the cross polar level).

Table 7. Angluar Resolution, ellipticity and depolarization factor for the FO ver5 coupled to the ALMA antenna and the feed models considered in this study.

	FWHM (max) arcmin	FWHM (min) arcmin	FWHM (average) arcmin	ellipticity	Depolarization
Gaussian W0 = 4mm					
67 GHz	1.43	1.46	1.45	1.019	0.70%
91.5 GHz	1.15	1.14	1.14	1.004	0.56%
116 GHz	0.90	0.91	0.91	1.005	0.38%
INAF Linear horn					
67 GHz	1.44	1.46	1.45	1.010	0.62%
91.5 GHz	1.12	1.13	1.12	1.009	0.35%
116 GHz	0.88	0.90	0.89	1.015	0.34%
INAF Profiled horn					
67 GHz	1.43	1.46	1.45	1.016	0.67%
91.5 GHz	1.09	1.11	1.10	1.019	0.38%
116 GHz	0.85	0.85	0.85	1.002	0.34%
IRAM profiled horn					
67 GHz	1.44	1.46	1.45	1.013	0.62%
91.5 GHz	1.12	1.12	1.12	1.004	0.39%
116 GHz	0.87	0.87	0.87	1.004	0.36%

9.3 ELECTROMAGNETIC MODEL OF THE CRYOSTAT WINDOW

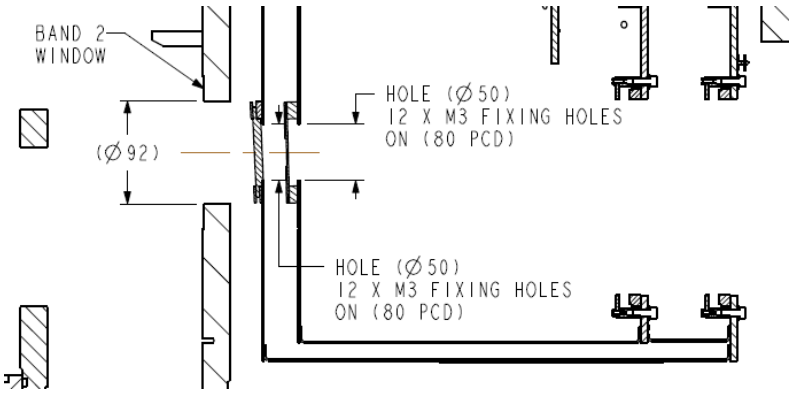

Figure 14: Detailed view of the windows and filters attached to the 110K and 15K cryostat shields.

To investigate the effect of the hole for window and filters we calculated the field in a near-field plane grid at the location of holes. This has been done using the **FO configuration Ver.5 with profiled INAF design**. We did not investigate here the overall EM effects of window and filter materials for which we refer to the IRAM study in the framework of this project.

Figure 16 and Figure 15 report the plots of the power pattern in the plane corresponding to the shields at 110K and 15K. Figure 17 reports the power pattern at window location. The pattern were calculated separately using PO/PTD technique and not in cascade. This means that the pattern Distribution at the 115K hole was evaluated neglecting any effect due to the 15K hole. In the same way the pattern distribution at the window was calculated neglecting the effects of the15K and 110K holes. From EM point of view this means that the pattern at the window does not take into account any truncation/diffraction effect due to the 15K and 110K filters.

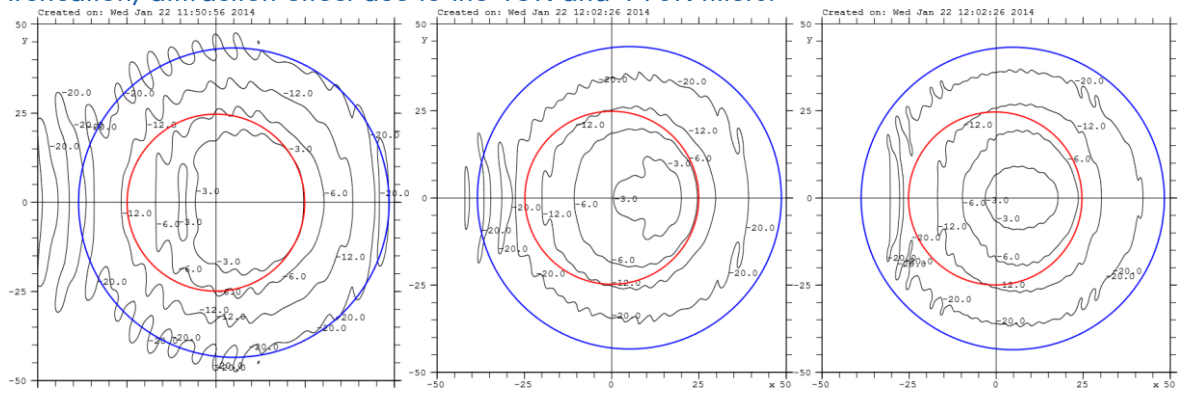

Figure 15: Power pattern at the 15K filter hole plane. The red circle is the 50mm hole as implemented for band 2 in the cryostat 15K shield. To guarantee pattern truncation at a level of -20 dB for the lowest frequency, a hole of 90 mm in diameter is needed. This is in line with the window hole diameter which is of 92 mm. 67 GHz; middle: 91.5 GHz; right: 116 GHz

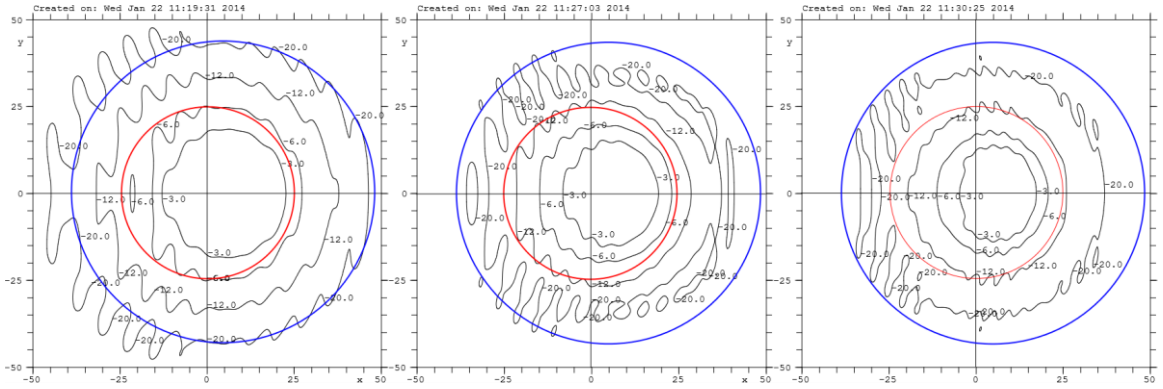

Figure 16: Power pattern at the 110K filter hole plane. The red circle is the 50mm hole as implemented for band 2 in the cryostat 110K shield. To guarantee pattern truncation at a level of -20 dB for the lowest frequency, a hole of 90 mm in diameter is needed. This is in line with the window hole diameter which is of 92 mm. Left: 67 GHz; middle: 91.5 GHz; right: 116 GHz

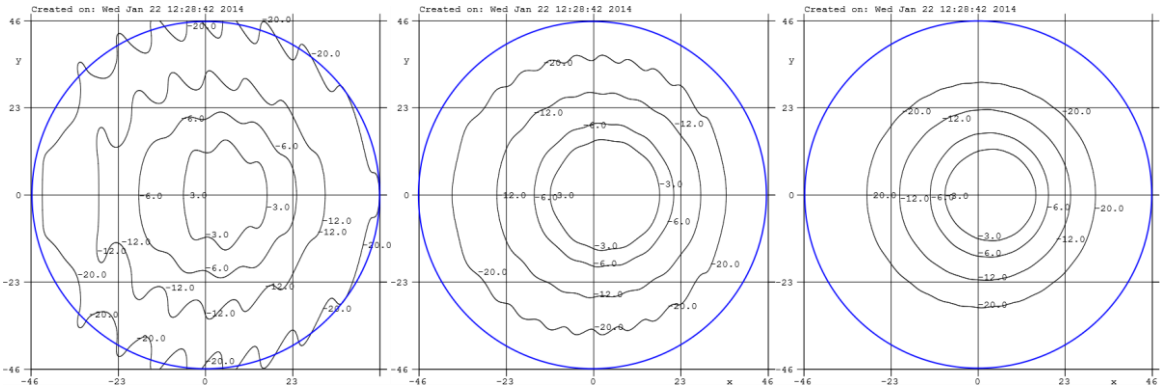

Figure 17: Power pattern at the window plane. The blue circle is the 92mm diameter hole as implemented for band 2 in the cryostat flange. 67 GHz; middle: 91.5 GHz; right: 116 GHz

It is readily seen that the diameter of the filter holes are too small compare with the diameter of the pattern, especially at lower frequency. A hole diameter of about 90mm is required to truncate the pattern at level of -20 dB from maximum. The location of the peak can be finely adjusted with further optimisations of the FO configuration.

9.4 Impact of feed designs

Different feed models has been used to calculated the performances of the fore-optics. Apart from the gsussian horn with a waist $w_0 = 4mm$ which has been used as the reference feed to design the FO, we used the electromagnetic model of feeds as developed within the ESO contract. The main goal was to investigate the effects of different electromagnetic designs based on specifications in [RD1].

They designs considered here for band 2+3 are:

1. INAF – OAA design
    a. Linear
    b. Profiled
2. IRAM design
    a. Dual profiled

The sketch of the designs are reported hereafter. See [6] and [7] for details on the designs.

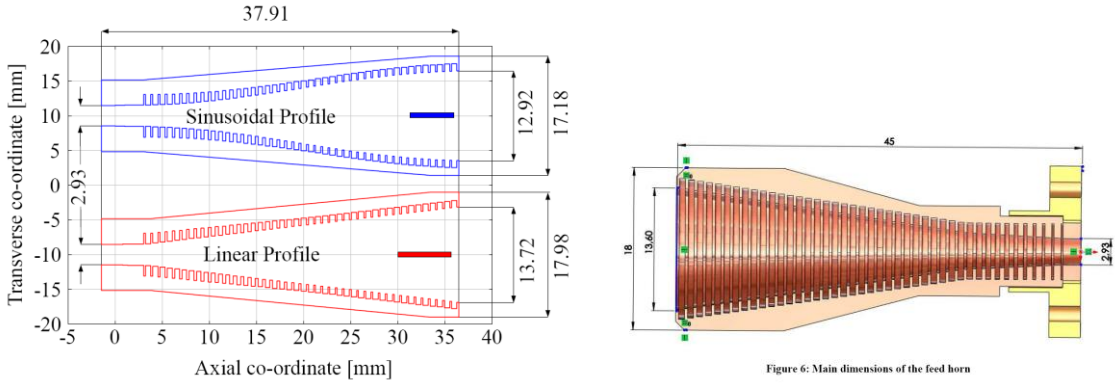

Figure 18: sketch of the three band 2+3 horns designed according to specifications. The INAF/OAA designs are on the left panel, the IRAM design is on the right.

While for the INAF design the EM model (i.e. amplitude and phase of the radiation pattern) was already delivered in GRASP format, for IRAM design a dedicated activity to calculate the radiation patterns was performed at IASF.bo. The geometry delivered by IRAM was inserted in the integral equations based **SRSR-D software**[1] and the radiation pattern were calculated and used as input in GRASP simulations.

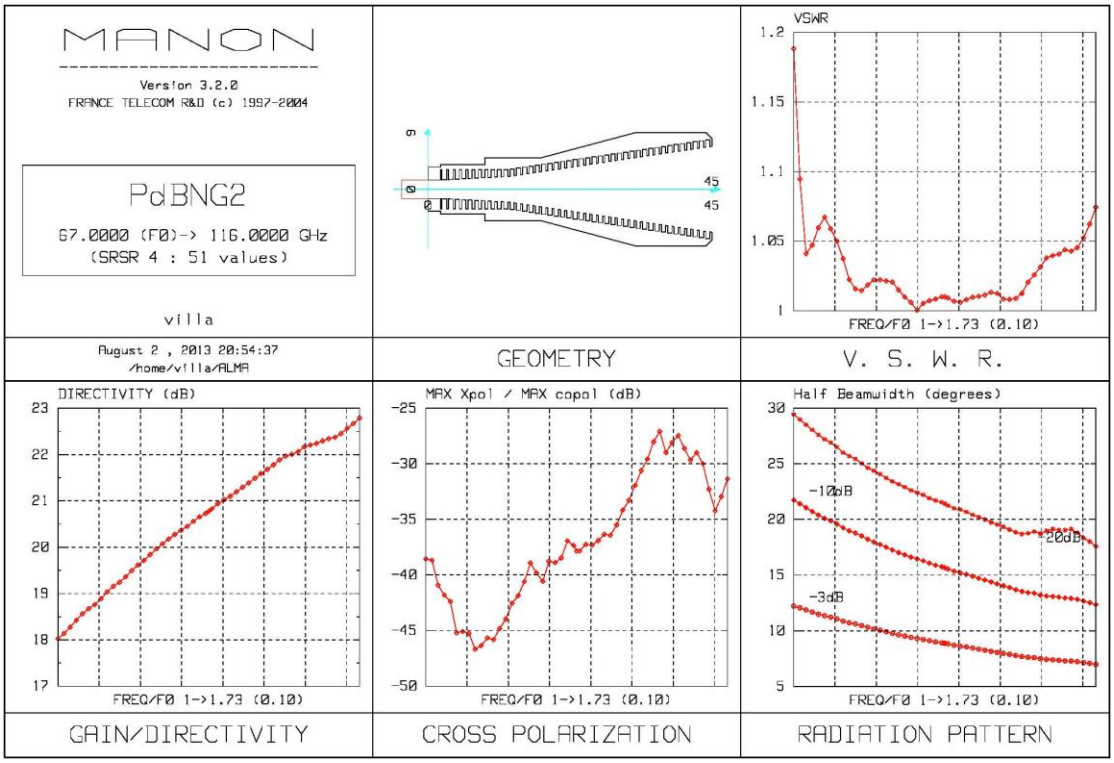

Figure 19. Overall performances of the IRAM feedhorn design as re-analysed at IASF to be used in FO GRASP simulations.

[1] SRSR-D software is a commercial software developed by ORANGE Telecom, France, R&D department.

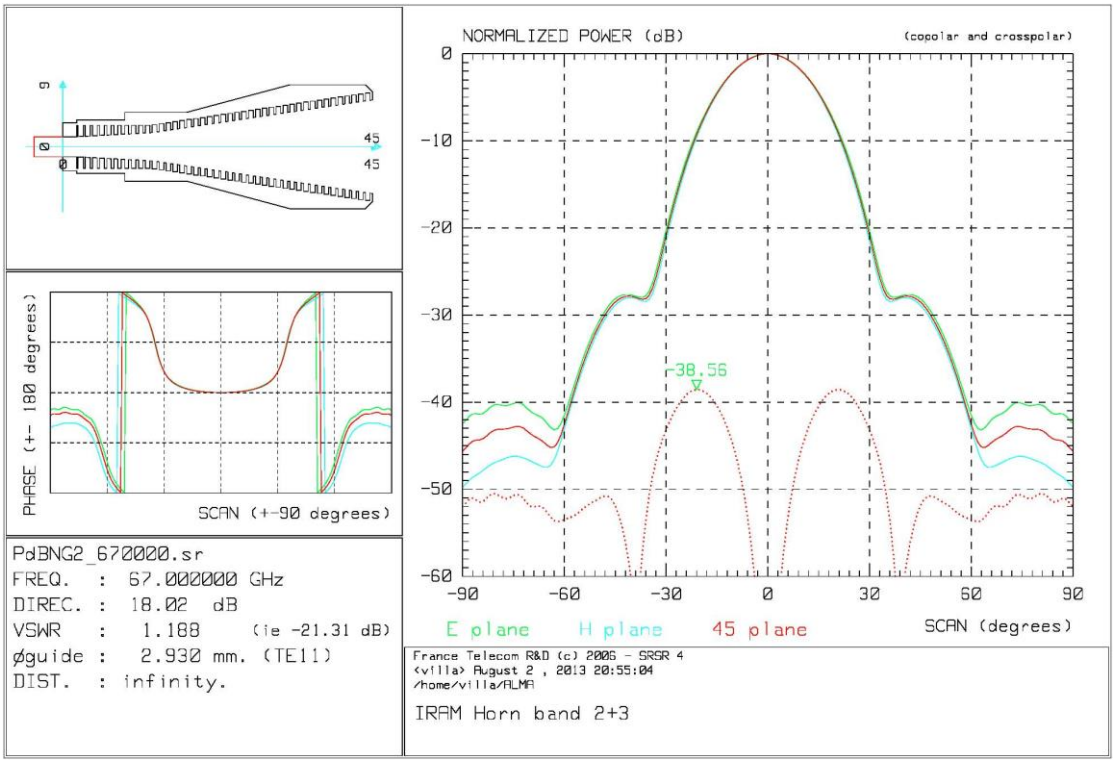

Figure 20. Radiation pattern of the IRAM horn design at 67.0 GHz

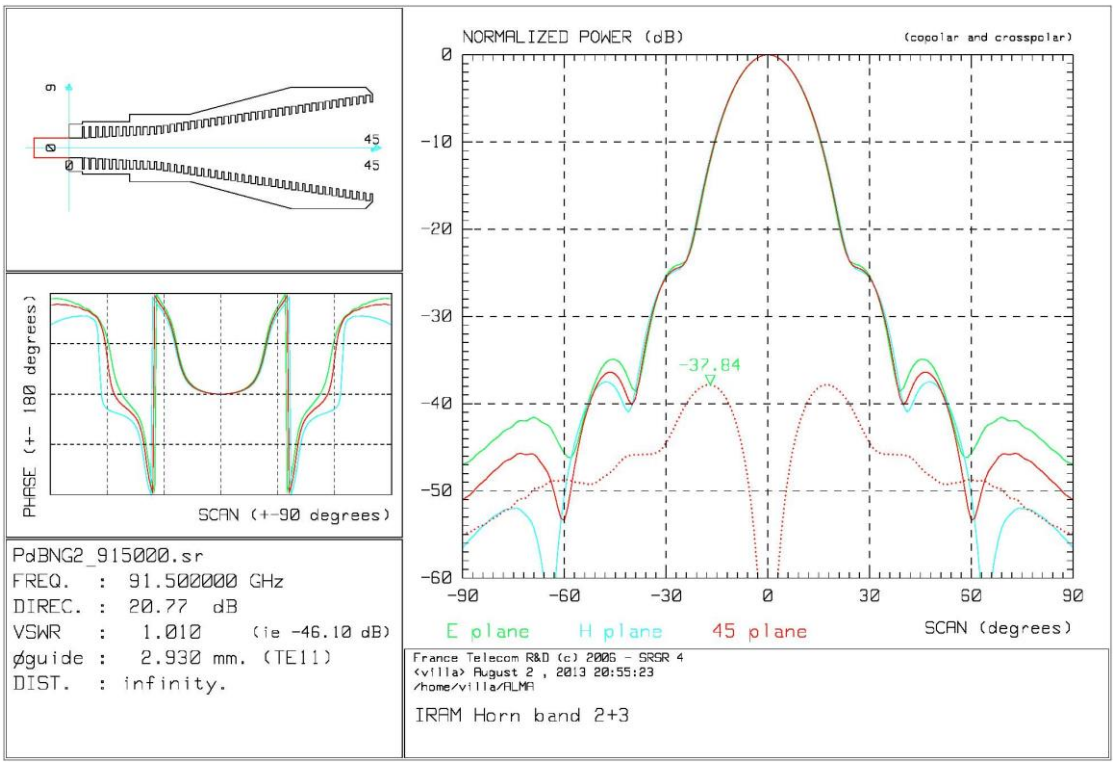

Figure 21. Radiation pattern of the IRAM horn design at 91.5 GHz

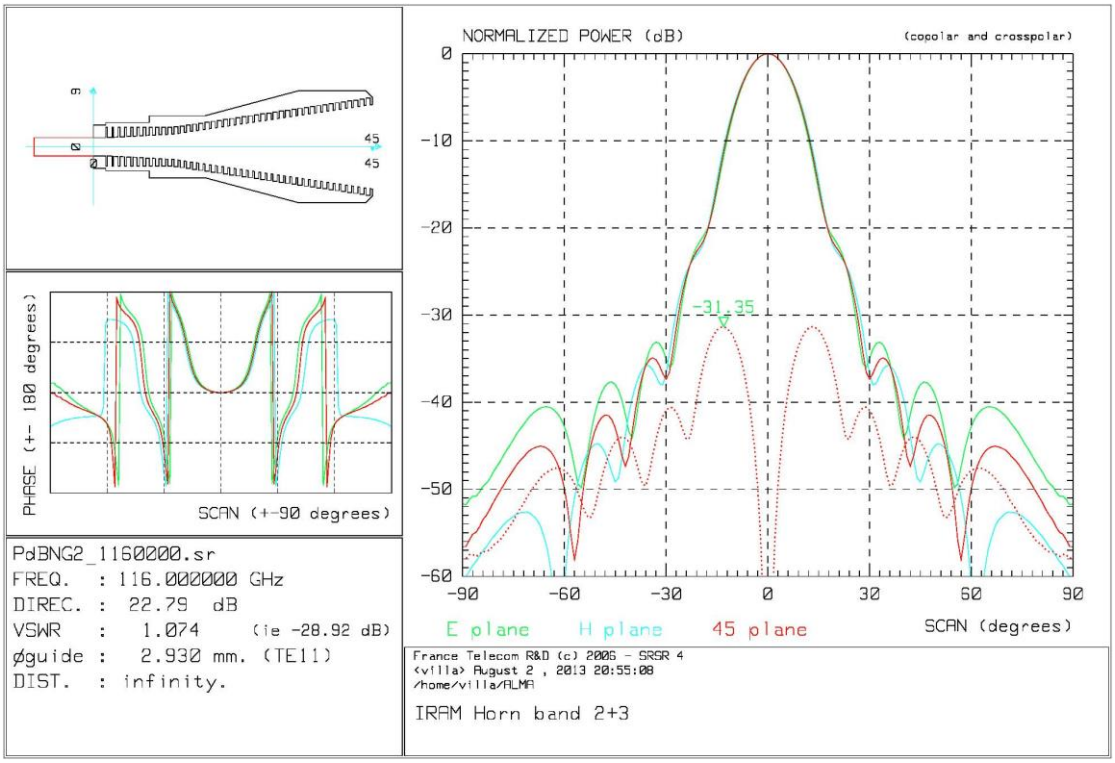

Figure 22. Radiation pattern of the IRAM horn design at 116.0 GHz

9.5 Fore Optics Ver5bis

This configuration is a slightly modification of the ver.5. The differences, as reported in Table 4 are due to the definition of focal length and curvature radii of the M2 mirror. Although there is no difference form mechanical point of view, this version has been analysed to evaluate the impact of a slightly different illumination of the secondary mirror. The calculated performances are reported in Table 8.

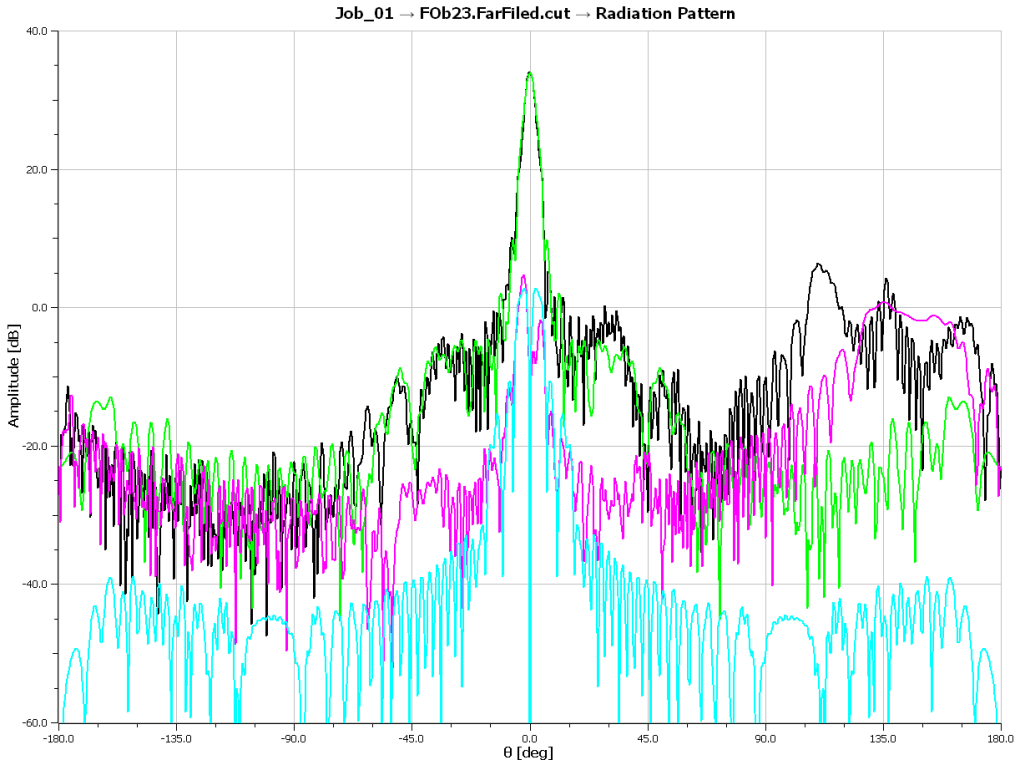

Figure 23. Far field radiation pattern @ 91.5 GHz of the Fore-Optics V5bis with INAF sin2 profiled horn. Black: E-plane copolar field; red: I-plane copolar field; green: H-plane copolar field; magenta: I-plane crosspolar field. Cyano: H-plane crosspolar field.

Table 8: Calculated parameters with fore-optics V5bis with INAF profiled horn design. The total efficiency includes also the illumination (in amplitude and phase) efficiency with respect to perfect uniform illumination function of the ALMA antenna.

Feed model	Directivity	Cross-polar Discrimination	Total and subreflector Spillover	Spill Efficiency	Pol+spill Efficiency	Total efficiency
INAF Profiled horn + FO ver5						
67 GHz	76.54 dBi	-26.92 dB	77.42% 78.76%	79.30%	79.05%	63.68%
91.5 GHz	79.12 dBi	-29.18 dB	78.47% 79.96%	79.42%	79.28%	61.80%
116 GHz	81.23 dBi	-32.25 dB	78.67% 80.58%	80.71%	80.57%	62.52%
INAF profiled horn + FO ver5bis						
67 GHz	76.54	-27.38	76.14% 77.49%	77.63%	77.41%	63.65%
91.5 GHz	79.17	-30.36	75.04% 76.55%	76.10%	76.00%	62.53%
116 GHz	81.41	-32.36	75.62% 77.35%	77.23%	77.11%	65.17%

10 CONFIGURATION 3: BAND3-LIKE WARM OPTICS

A study of the beam propagation through the ALMA train of mirrors has been done using Quasi-Optical techniques [9].
The ALMA mirror configuration here considered is the Cassegrain configuration (Hyperboloid and Paraboloid) whose geometry has been taken by [1] and two different re-focusing systems: the first one, which is here referred to as the **Warm Optics**, can be considered as the baseline design for band 3, detailed in [10] and [11], and shown in Figure 24; the second one has been studied and developed in the present framework and is here referred to as the **Cold Optics Ver5**.

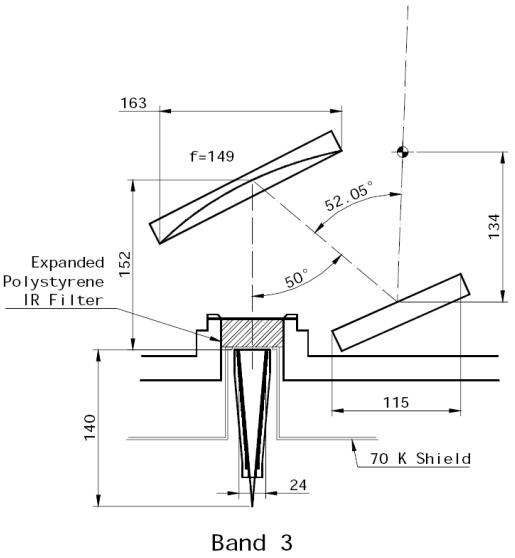

Figure 24: Geometry of the Band 3 Warm Optics re-focusing system (From [1])

Although the Warm Optics was designed to cover the 84-116GHz band (the nominal band 3 of ALMA) the analysis has been extended to the joint band 2+3 (67-116GHz) to study its behavior in this enhanced bandwidth, where the feasibility study of a receiver was addressed in this project. The Cold Optics was instead directly designed in band 2+3.
Another aspect of the study to point out is that the Warm Optics has been located in the originally allocated band 3 position outside the top of the ALMA cryostat; differently, the Cold Optics has been developed with the aim to be placed inside the cryostat within the ALMA cartridge in the space originally reserved to the ALMA band 2. The two positions (detailed in [1]) are however not significantly different to each other.
From the feed horn point of view the optical systems require different beam features and thus different corrugated horns have been used in the analysis; In the Warm Optics it has been used the feed given in [7] while in the Cold Optics the **INAF Profiled design** has been used. In both cases the feed is the optimum design for the Optics. The only information needed, as regards feed performance, for this Quasi-Optical kind of comparative study is the beam waist and its position and these properties are a sort of input to the performance budget, given in the first row of Table 9. The beam waist is directly given while its position is calculated with respect to the center of the feed aperture.
Another important difference between the two re-focusing optical systems is that the couple of mirrors of the Warm Optics is formed by one planar and one elliptical mirror while in the case of the Cold Optics mirrors are both elliptical. To better figure out the quasi-optical beam propagation through the

mirrors two different sketches are given: the first, shown in Figure 25, refers to the Warm Optics, while the second, in Figure 26, to the Cold Optics.
The performance breakdown listed in Table 9 refers to the geometrical and optical properties drawn in Figure 25 and Figure 26.
The two mirrors of re-focusing are numbered starting from the feed while the Hyperboloid and the Paraboloid are indexed by pedex H and P (respectively).
The relative position of the mirrors is indicated by d_{ij}. It represents the length of the optical path, through the beam axis between Mirror i and j, hitting each mirror in what in Errore. L'origine riferimento non è stata trovata. is named Vertex. Pedex $i = 0$ is associated to the (Waist position of the) feed.

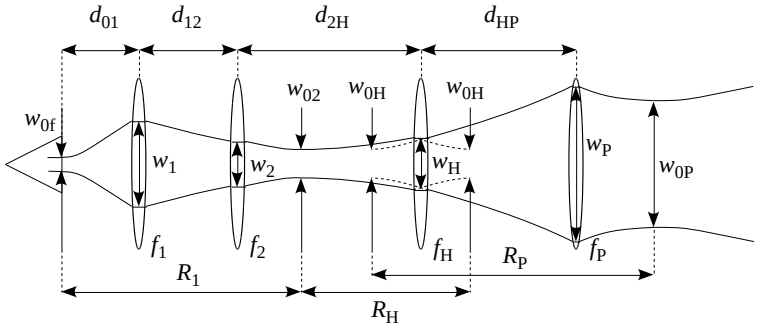

Figure 25: Beam-propagation reference-sketch for Quasi-Optical analysis of the Warm Optics configuration including ALMA antenna.

Fundamental Mode Gaussian Beam is used to characterize wave propagation between subsequent mirrors. When the wave propagation direction is known, a single Gaussian Beam is fully determined by specifying its Beam Waist w_{0i} (between Mirror i and $i + 1$) and beam waist position. Each Mirror i acts as a Beam transformer, through the Effective Focal Length f_i, and, if the Beam Waist and its position is known somewhere (in this case at the feed), a model based on simple analytical formulas can be used to predict wave propagation through an arbitrary train of mirrors [9]. The formulas that rule the transformation between two Fundamental Mode Gaussian Beams across Mirror i are based on the knowledge of the curvature of the phase and Beam Radius w_i at that mirror. It has to be noticed that in the Warm Optics scheme, since Mirror 2 is planar, there is no Beam Waist between Mirror 1 and 2, the Gaussian Beam keeps unchanged crossing Mirror 2 and there is one only Beam Waist from Mirror 1 to H (located between Mirror 2 and H).
A sensitive study has been done also as regards the defocusing of the feed in the focal position of the Cold Optics ver5 configuration. Results for a **6 mm displacement** from the focal point are given in red as second entry in Errore. L'origine riferimento non è stata trovata..

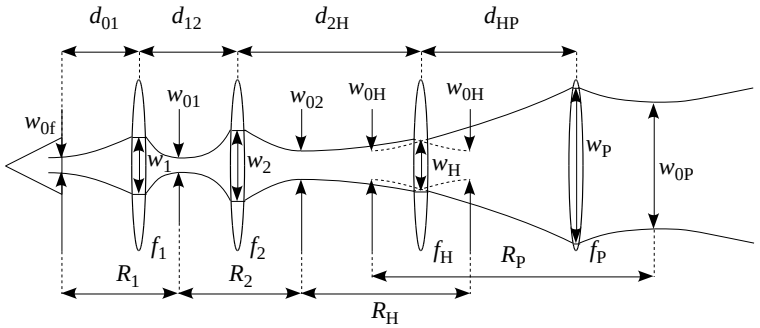

Figure 26: Beam-propagation reference-sketch for Quasi-Optical analysis of the Cold Optics configuration (ver.5) including ALMA antenna.

The distance between two subsequent waist positions across Mirror i is indicated as R_i. Please note that in the case of the Hyperboloid Mirror (Figure 25 and Figure 26) the virtual waist doubles its position according to what side is considered (the waist position is always at the back side of the Hyperboloid).

The angular resolution values reported in Table 9 are derived from an estimation of the angular extend of the -3dB contour level; they are slightly different from numbers reported in Table 6 which are calculated from a gaussian fit in the all angular region of the PO/PTD beam calculation.

Table 9: ALMA band 2/3 Optical budget: Comparison between Warm and Cold Optics. Red entries are related to 6 mm defocusing.

	Warm Optics (Baseline)			Cold Optics ver5		
Optical/Geometrical Feature	**67 GHz**	**91.5 GHz**	**116 GHz**	**67 GHz**	**91.5 GHz**	**116 GHz**
Waist at feed (w_f) [mm]	7.40	7.15	6.85	3.73	3.99	4.10
Waist position relative to feed aperture [mm]	-11.48	-19.99	-29.56	-0.53	-1.57	-5.25
Feed to Mirror 1 path length (d_{01})[mm]		152.7			50, 56	
Mirror 1						
Type		Ellipsoid			Ellipsoid	
Focal Length (f_1) [mm]		149.09			25	
Rim Axes† (Max, Min) [mm]		160, 140			40	
Beam Radius at Vertex of Mirror (w_1) [mm]	30.33	23.41	19.57	19.47, 21.71	13.68, 15.19	10.85, 11.98
Rim Mean Diameter‡ over Beam Radius ratio	5.01	6.49	7.77	2.05, 1.84	2.92, 2.63	3.69, 3.34
Spillover Efficiency†† [%]	98.71	99.42	99.69	90.45, 85.17	93.76, 92.43	94.95, 92.59
Mirror 1 to Mirror 2 path length (d_1)[mm]		169.79			140	
Mirror 2						
Type		Plane			Ellipsoid	
Focal Length (f_2) [mm]		∞			89.9	
Rim Axes (Max, Min) [mm]		120, 112			78.73, 72.86	
Beam Radius at Vertex of Mirror (w_2) [mm]	24.46	19.57	16.81	38.44, 48.10	29.86, 35.83	26.12, 30.23
Rim Mean Diameter over Beam Radius ratio	4.74	5.93	6.90	1.97, 1.58	2.54, 2.12	2.90, 2.51
Spillover Efficiency [%]	99.12	99.78	99.89	88.31, 86.28	92.35, 88.18	90.52, 86.28
Mirror 2 to Mirror 3 path length (d_{2H})[mm]		6007.22			6118	
Mirror H						
Type				Hyperboloid		
Focal Length (f_H) [mm]				-311.59		
Rim Axes (Max, Min) [mm]				750		
Beam Radius at Vertex of Mirror (w_H) [mm]	348.9	315.2	287.6	239.8, 263.7	255.0, 265.8	261.5, 267.8
Rim Mean Diameter over Beam Radius ratio	2.15	2.38	2.61	3.13, 2.84	2.94, 2.82	2.87, 2.80
Spillover Efficiency [%]	94.67	96.43	96.65	87.03, 87.69	92.67, 91.48	90.11, 89.91
Mirror 3 to Mirror 4 path length (d_{HP}))[mm]				4506		
Mirror P						
Type				Paraboloid		
Focal Length (f_P) [mm]				4800		
Rim Axes (Max, Min) [mm]				12000		
Beam Radius at Vertex of Mirror (w_P) [mm]	5.656	5.109	4.663	3.893, 4.297	4.142, 4.325	4.248, 4.355
Rim Mean Diameter over Beam Radius ratio	2.12	2.35	2.57	3.08, 2.79	2.90, 2.77	2.82, 2.76
Spillover Efficiency [%]	98.54	98.84	98.98	98.15, 98.24	98.28, 98.21	97.65, 97.72
Other Relevant Parameters						
Inter-waist distance of Mirror 1 (R_1) [mm]	449.4	420.3	409.0	96.69, 99.34	93.23, 97.24	90.02, 95.08
Waist Between Mirror 1 and 2 (w_{01}) [mm]	Not Defined (Planar Mirror)			3.47, 2.87	3.4, 2.89	3.17, 2.76
Inter-waist distance of Mirror 2 (R_2) [mm]	Not Defined (Planar Mirror)			513.4, 877.9	512.1, 692.4	513.8, 621.0
Waist Between Mirror 2 and H (w_{02}) [mm]	23.43	19.11	16.57	34.22, 29.09	23.44, 21.76	18.00, 17.25
Inter-waist distance of Mirror H (R_H) [m]	6.188	6.226	6.247	5.994, 5.631	5.998, 5.819	6.000, 5.893
Waist‡‡ Between Mirror H and P (w_{0H}) [mm]	1.21	0.981	0.848	1.76, 1.59	1.21, 1.16	0.93, 0.908
Inter-waist distance of Mirror P (R_P) [km]	8.548	8.850	8.980	5.189, 3.858	8.172, 8.791	10.26, 11.30
Waist Between Mirror P and sky (w_{0P}) [m]	2.37	1.96	1.70	3.04, 4.08	2.76, 3.35	2.42, 2.76
From Physical Optics Analysis						
Total Spillover Efficiency of Mirror train [%]	91.27	94.55	95.27	68.24, 60.04	78.86, 73.23	75.63, 70.19
Antenna Directivity [dBi]	77.3	80.0	81.8	76.1, 75.5	79.1, 78.6	80.9, 80.6
Cross-polarization [dBi]	49.9	51.7	53.7	48.7, 47.4	50.1, 49.1	48.2, 48.7
Boresight Angle (from antenna axis) [arcsec]	399.8	398.0	397.3	552.6, 553.6	554.4, 555.7	555.8, 556.1
FWHM [arcsec]	93.18	64.16	49.13	89.28, 88.94	71.28, 70.31	54.72, 54.21
Side Lobe Level [dB]	–23.1	-19.0	-27.6	-18.8, -19.1	-25.5, -27.0	-29.0, -28.9

† In general the Mirror Rim is a planar ellipse, in particular cases it is a circle; Major and Minor axes are given in the general case; only the circle diameter is given in the particular case.

‡ The Mean Diameter is the mean between the major and the minor axis of the rim ellipse. In the case of the prime and secondary ALMA mirrors the rim is a circle and the Mean Diameter is the circle diameter.

†† The Spillover Efficiency is the percentage of incident power hitting the mirror. It is calculated from Physical Optics analysis.

‡‡In this case the waist is 'virtual' since the mirror is an Hyperboloid and the beam does not travel through the waist

11 OTHER SOLUTIONS

There are other possibilities that can be investigated, both at cold and at ambient temperature. Apart from the use of conventional lenses together with mirrors, within this project it was also taken into account the possibility to develop a Fore-Optics based on planar mesh lenses. The concept has been demonstrated through measurements on a F/3 lens prototype at W-band using photolithographic techniques [3]. However the use of a planar lens has not been addressed in this study and still remains as an open option.

12 Conclusions for the Final Review

A preliminary study of the Fore-Optics system for the band 2+3 cartridge has been proposed. The intent of this study was mainly to investigate the possibility to design a optics system at cold, i.e. to be located inside the cryostat. The optical layout is based on a two ellipsoidal off-axis system. Alternatively the fore-optics configuration already implemented in the band 3 ALMA cartridge has been analysed also for the band 2+3 system.
Several configuration were studied and the most suitable resulted the configuration ver.5 both in term of mechanical envelope and performances. Based on this design, a configuration named ver.5bis (with a slightly modified parameters of the M2 mirror) was also analysed and compared. Hereafter we report some consideration derived from the study presented.

Advantages of the cold optics.
The advantage to implement a cold optics for band 2+3 is both in terms of added noise and stability. This has been reported in Chapter 7. The noise added by a cold optics is approx. 1 order of magnitude lower that the noise added by a warm optics (0.06K instead of 0.6K). The cold optics offer superior performances in terms of thermal stability since it is located in a controlled environment. This means that the contribution to the signal due to temperature fluctuations is negligible at cold, while can be of few mK (for a 2K of ambient temperature variation) if the optics is at warm temperature.

Disadvantages of the cold optics.
The main drawback is the RF interface of the cold optics with the holes in the cryostat. While the hole window clearance seems to be appropriate to guarantee the required illumination of the sub-reflector, the holes in the cryostat 110K and 15K shields seems to be too small at all frequencies between 67 and 116 GHz. The truncation of the pattern due to the filters should be carefully evaluated but for a preliminary analysis assessed here a hole of 90mm (instead of 50mm as in the actual design) in diameter is more appropriate. At this time the main problem towards the implementation of a cold optics is the change of the filter holes in the sield.

RF performances.
There are no substantial differences between the cold optics (band 2+3 ver.5) and warm optics (band 3) from performance point of view. For both configurations in this frequency range is hard to guarantee a 5waist truncation diameter as required by ALMA. In terms of spillover the performances at these frequency are worse than in other bands. In this respect a cold optics can perform better than a warm optics since all the spillover energy form FO mirrors see an ambient at cryogenic temperature and the contribution to the antenna temperature is reduced. At **67 GHz** the effect of the truncation is **1.8K** to be compared with **1.4K** as specified for band 2 [3]. At **116 GHz** the truncation effect is **0.3 K** compared to **0.1 K** as specified for band 3 [3]. Even if the obtained values are outside specifications, there is still margin of optimization.

Efficiency.
The efficiencies reported in Table 6 for different horn models coupled with FO and in Table 4 for reference configurations, show that it is hard to reach specified efficiency as reported in table IX of [1] in this very-wide frequency range. A dedicated study to revise efficiency budget together with noise budget derived from optics as a function of frequency and ALMA top-level specification is warmly suggested.

Feed design.

Although INAF profiled design offer a slightly better overall efficiency performances (both in terms of efficiency values and stability with frequency), there is no dramatic dependence of the FO performances with corrugation profile. We would stress however that an iteration of the feed location w.r.t FO has not performed. A preliminary sensitivity analysis demonstrated that a feed shift of 6 mm (i.e. 1.34 λ at the lower frequency) gives a change in directivity and cross polar level of about 1dB or less and a change in the total spillover efficiency of about 5% - 8%.

13 REFERENCES

[1] J. Lamb, A. Baryshev, Carter, M.C., L. D'Addario, G. W. Ellison B.N., B. Lazareff, Y. Sekimoto e C. Tham, «ALMA Receiver Optics Design,» *ALMA Memo Series,* n. 362, 2001.

[2] F. Villa, «ALMA fore-optics and feed horn specification requirements,» 2012.

[3] M. Carter, B. Lazareff, S. Navarro, A. Baryshev, M. Harman, J. Lamb, G. Ediss, C.-Y. Tham, Y. Sekimoto, M. Matsunaga, V. Heinz e F. Patt, «ALMA Front-end Optics Design Report - FEND-40.02.00.00-035-B-REP,» ALMA report, 2007.

[4] J. W. Lamb, «Low-Noise, High efficiency optics design for ALMA receivers,» *IEEE Trans. on Antennas and Propagations,* vol. 51, n. 8, p. 2035, 2003.

[5] K. Pontoppidan, "Electromagnetic properties and optical analysis of the ALMA antennas and Front Ends," TICRA, 2008.

[6] R. Hill, «Calculatioion of Efficiencies, etc, from beam scanning data,» ALMA internal note, 2008.

[7] R. Nesti, «ALMA Band 2/3 WP4: Passive Components 1 - Feedhorns - Electromagnetic Study,» Arcetri Observatory Internal Report, Arcetri, 2013.

[8] A.-L. Fontana, «ALMA B2+3; WP4: Feed horn design,» 2013.

[9] D. H. Martin e J. W. Bowen, «Long-wave Optics,» *IEEE trans. Antennas Propagat.,* vol. AP.41, n. 10, pp. 1676-1690, 1993.

[10] J. Lamb, «Optics Study for ALMA Receivers,» *ALMA Memo Series,* n. 359, 2001.

[11] Lamb, J., «Optimized Optical Layout for MMA 12-m Antennas,» *MMA Memo Series,* n. 246, 2001.

[12] G. Pisano, M. Wah Ng, F. Ozturk, B. Maffei e V. Haynes, Dielectrically embedded flat mesh lens for millimeter waves applications, vol. 52, Applied Optics, 2013, pp. 2218 - 2225.

[13] Y. T. Lo e S. Lee, Antenna Handbook Vol. 2: Theory, Van Nostrand Reinhold, 1993.

[14] R. Nesti, «ALMA band 2/3 WP4: Passive components I - Feedhorns - Electromagnetic Study,» n. 4, 2013.